

Reconstruction of inclusions in an elastic body

Gunther Uhlmann^{a,*}, Jenn-Nan Wang^{b,2}, Chin-Tien Wu^{c,3}

^a Department of Mathematics, University of Washington, Box 354305, Seattle, WA 98195-4350, USA

^b Department of Mathematics, Taida Institute for Mathematical Sciences, and NCTS (Taipei), National Taiwan University, Taipei 106, Taiwan

^c Department of Applied Mathematics, National Chiao Tung University, Hsinchu 300, Taiwan

Received 22 October 2008

Available online 17 January 2009

Abstract

We consider the reconstruction of elastic inclusions embedded inside of a planar region, bounded or unbounded, with isotropic inhomogeneous elastic parameters by measuring displacements and tractions at the boundary. We probe the medium with complex geometrical optics solutions having polynomial-type phase functions. Using these solutions we develop an algorithm to reconstruct the exact shape of a large class of inclusions including star-shaped domains and we implement numerically this algorithm for some examples.

© 2009 Elsevier Masson SAS. All rights reserved.

Résumé

On considère le problème de la reconstruction des inclusions dans un domaine élastique plan borné ou non borné, les paramètres élastiques, supposés isotropes et non homogènes, sont déterminés à partir de mesures de déplacements et de tractions à la frontière du domaine. On teste le milieu en utilisant des solutions de l'optique géométrique complexe dont les fonctions de phase sont de type polynomial. En utilisant ces solutions on développe un algorithme de reconstruction de la forme exacte d'une classe importante d'inclusions contenant les domaines étoilés ; on implémente numériquement cet algorithme dans quelques exemples.

© 2009 Elsevier Masson SAS. All rights reserved.

MSC: 35R30; 74B05

Keywords: Reconstruction of inclusions; Complex geometrical optics; Numerical algorithms of reconstruction

1. Introduction

The purpose of this paper is several fold. First, we provide numerical evidence for the algorithms developed in [19] and [20] for determining elastic inclusions embedded in an inhomogeneous background. Second we extend, and simplify, the object identification result in [16] from the conductivity equation on an infinite slab to the elasticity

* Corresponding author.

E-mail addresses: gunther@math.washington.edu (G. Uhlmann), jnwang@math.ntu.edu.tw (J.-N. Wang), ctw@math.nctu.edu.tw (C.-T. Wu).

¹ Supported in part by NSF and a Walker Family Endowed Professorship.

² Supported in part by the National Science Council of Taiwan (NSC 96-2628-M-002-009).

³ Supported in part by the National Science Council of Taiwan (NSC 96-2115-M-009-014).

system. Third we also develop a numerical algorithm for the case of the infinite slab and we test it numerically. Our main method is to use complex geometrical optics (CGO) solutions with general phases constructed in [20] to treat the inverse problems.

We consider the problems in the plane. Let Ω be an open domain in \mathbb{R}^2 with smooth boundary $\partial\Omega$ which is not necessarily bounded. The domain Ω is filled with an inhomogeneous, isotropic, elastic medium characterized by the Lamé parameters $\lambda(x)$ and $\mu(x)$. Assume that $\lambda(x) \in C^2(\overline{\Omega})$, $\mu(x) \in C^4(\overline{\Omega})$ and the following inequalities hold:

$$\mu(x) > 0 \quad \text{and} \quad \lambda(x) + 2\mu(x) > 0 \quad \forall x \in \overline{\Omega} \quad (\text{strong ellipticity}). \quad (1.1)$$

We consider the static isotropic elasticity system without sources:

$$\mathcal{L}u := \nabla \cdot (\lambda(\nabla \cdot u)I + 2\mu S(\nabla u)) = 0 \quad \text{in } \Omega. \quad (1.2)$$

Here and below, $S(A) = (A + A^T)/2$ denotes the symmetric part of the matrix $A \in \mathbb{C}^{2 \times 2}$. Equivalently, if we denote $\sigma(u) = \lambda(\nabla \cdot u)I + 2\mu S(\nabla u)$ the stress tensor, then (1.2) becomes:

$$\nabla \cdot \sigma = 0 \quad \text{in } \Omega.$$

On the other hand, since the Lamé parameters are differentiable, we can also write (1.2) in the nondivergence form:

$$\mu \Delta u + (\lambda + \mu) \nabla(\nabla \cdot u) + \nabla \lambda \nabla \cdot u + 2S(\nabla u) \nabla \mu = 0 \quad \text{in } \Omega. \quad (1.3)$$

Recently, a framework of constructing CGO solutions with general phases for systems with the Laplacian as the leading part was proposed by the first two authors [20]. The elasticity system (1.2) is among the systems considered in [20]. To simplify the presentation, we will not go over the development of CGO solutions and their important role in inverse problems. For more details, we refer to [17,18] and references therein.

To really appreciate the usefulness of CGO solutions with general phases, we shall study the inverse problem with an unbounded background domain. Ikehata in [10] considered the inverse conductivity problem in an infinite slab where the location of an inclusion is reconstructed by infinitely many boundary measurements. In [10], he used Calderón type harmonic functions [4], i.e., $e^{x \cdot (\omega + i\omega^\perp)}$ with $\omega \in \mathbb{S}^{n-1}$. These functions are not integrable on hyperplanes. To remedy this, he introduced Yarmukhamedov's Green function to construct a sequence of harmonic functions with finite energy that approximate the Calderón type function on a bounded part of the slab and are arbitrarily small on an unbounded part of the slab.

In [16] the authors used complex spherical waves rather than Calderón type functions for the object identification problem in the slab. The most obvious advantage is that they do not need Yarmukhamedov's Green function to "localize" complex spherical waves since these solutions decay faster than any given polynomial order on infinite hyperplanes. In this work, we extend the result in [16] to the elasticity system (1.2). We also simplify some arguments in [16]. Likewise, we consider the object identification problem in an infinite strip. As in [20], we will use CGO solutions with phases being complex polynomials. For these solutions, the probing fronts are confined in a suitable cone. By increasing the degree of the polynomial, one can shrink the opening angle of the cone and, therefore, squeeze the probing fronts. We remark that the probing fronts of complex spherical waves are spheres or circles. In other words, we are able to determine more information of the unknown object using CGO solutions with polynomial phases.

For the reconstruction of the unknown object in two dimensions, we would like to mention an interesting result by Ikehata in [11] where he introduced the Mittag-Leffler function in his method. The numerical implementation of [11] was carried out by Ikehata and Siltanen in [12]. However, the approach with the Mittag-Leffler function cannot be applied to the isotropic elasticity system with inhomogeneous medium.

To put this work in perspective, we would like to mention another reconstruction method for the elasticity system developed by Ikehata [8], which is called the probe method. The ideas of the probe method came from Isakov's fundamental work [13]. The probe method uses singular solutions (or the fundamental solution) to do the reconstruction. A key ingredient of the probe method is a Runge type approximation theorem which guarantees the existence of an approximating sequence to the singular solution. The boundary conditions of the approximating sequence characterize the input data needed for reconstruction. However, in general, a Runge type approximation theorem is not constructive. That is, to actually characterize the needed input data is problematic. Therefore, it is hard to numerically realize the probe method, at least, for the elasticity. Our method uses CGO solutions which are globally defined in a bounded domain. We do not need a Runge type theorem. The boundary conditions of the CGO solutions are exactly the input data for reconstruction.

For imaging elastic inclusions by boundary measurements, we would like to mention an effective method developed by Ammari and Kang’s group. They assume that the size of inclusion is small and the background medium is homogeneous. Using layer potential techniques, a full asymptotic expansion of the displacement field in the order of the size of inclusion can be derived [2]. The most important quantities in the expansion are so-called elastic moment tensors. These elastic moment tensors contain significant information of the inclusion and its medium properties. Some numerical results based on this method was reported in [14]. For more detailed development of this method for imaging small inclusions, we refer the reader to Ammari and Kang’s book [1].

Another interesting related topic is the imaging problem for the quasi-incompressible elasticity in which $\lambda \gg \mu$. The quasi-incompressibility assumption is valid for the biologic tissues. Therefore, it is widely used in the magnetic resonance elastography (MRE). MRE is an approach aiming to determine the material properties by interior measurements. Recently, a new method based on the assumption of small inclusions was proposed by Ammari et al. [3]. In this method, the quasi-incompressible elastic system is approximately by a sequence of nonhomogeneous modified Stokes system. Similar to the elastic moment tensors, the information of the shape of the elastic anomaly and its shear modulus is contained in the viscous moment tensors which appear in the expansions of the displacement field. Our method can also used to image inclusions for the quasi-incompressible elasticity in the plane when it is approximated by the Stokes system. In [5], we consider the reconstruction of the obstacle for the Stokes system with inhomogeneous medium coefficients in three dimensions using complex spherical waves. It is rather easy to extend the result of [5] to the case of reconstructing inclusions in two dimensions using our new complex geometrical optics solutions. It is an interesting project to explore the possibility of determining the material properties of inclusions by our method.

This paper is organized as follows. In Section 2, we show how to construct CGO solutions with general phases for the elasticity system. In Section 3, we apply these CGO solutions to study the reconstruction of inclusions by boundary measurements and give a numerically feasible algorithm. In Section 4, we provide some computational results with simulated data.

2. CGO solutions with general phases for the elasticity system

In this section we recall the construction of CGO solutions to (1.2) outlined in [20]. To do so, we first reduce the system to the one with the Laplacian as the leading part. We will use the reduced system derived by Ikehata (see for instance [9,17]). Let $\begin{pmatrix} w \\ g \end{pmatrix}$ satisfy:

$$\Delta \begin{pmatrix} w \\ g \end{pmatrix} + A(x) \begin{pmatrix} \nabla g \\ \nabla \cdot w \end{pmatrix} + Q(x) \begin{pmatrix} w \\ g \end{pmatrix} = 0, \tag{2.1}$$

where

$$A(x) = \begin{pmatrix} 2\mu^{-1/2}(-\nabla^2 + \Delta)\mu^{-1} & -\nabla \log \mu \\ 0 & \frac{\lambda+\mu}{\lambda+2\mu}\mu^{1/2} \end{pmatrix},$$

and

$$Q(x) = \begin{pmatrix} -\mu^{-1/2}(2\nabla^2 + \Delta)\mu^{1/2} & 2\mu^{-5/2}(\nabla^2 - \Delta)\mu\nabla\mu \\ -\frac{\lambda-\mu}{\lambda+2\mu}(\nabla\mu^{1/2})^T & -\mu\Delta\mu^{-1} \end{pmatrix}.$$

Here $\nabla^2 f$ is the Hessian of the scalar function f . Then

$$u := \mu^{-1/2}w + \mu^{-1}\nabla g - g\nabla\mu^{-1} \tag{2.2}$$

satisfies (1.3).

Now let Ω_0 be a suitable subdomain of Ω and $\rho(x) = \varphi(x) + i\psi(x)$ be conformal in Ω_0 . Moreover, we assume that $\rho(x)$ is a diffeomorphism in Ω_0 . Then we can find $U(x)$ satisfying (2.1) in Ω_0 with

$$U(x) = \begin{pmatrix} w \\ g \end{pmatrix} = e^{(\varphi+i\phi)/h}(L + R), \tag{2.3}$$

for some three-dimensional vectors L and R , where L is independent of h and R satisfies:

$$\|\partial^\alpha R\|_{L^2(\Omega_0)} \leq Ch^{1-\alpha}, \quad \forall |\alpha| \leq 2. \tag{2.4}$$

Our method of constructing $U(x)$ in the form (2.3) goes as follows. Let (y_1, y_2) be the new coordinates defined by $y_1 = \varphi(x)$ and $y_2 = \psi(x)$. In the new coordinates (y_1, y_2) , (2.1) is transformed into

$$\Delta \begin{pmatrix} \tilde{w} \\ \tilde{g} \end{pmatrix} + \tilde{A}(y, D) \begin{pmatrix} \tilde{w} \\ \tilde{g} \end{pmatrix} + \tilde{Q}(y) \begin{pmatrix} \tilde{w} \\ \tilde{g} \end{pmatrix} = 0, \tag{2.5}$$

where $\tilde{A}(y, D)$ is a first order differential operator. Using the Carleman technique or the method of intertwining operators [15], one can construct CGO solutions to (2.5) with linear phases, namely,

$$\tilde{U}(y) = \begin{pmatrix} \tilde{w} \\ \tilde{g} \end{pmatrix} = e^{(y_1 + iy_2)/h} (\tilde{L} + \tilde{R}).$$

Then to get (2.3), we simply make a change of coordinates $y \rightarrow x$, i.e. $U(x) = \tilde{U}(y(x))$ (see [20] for more details). The key idea in this approach is that the Laplacian is invariant under conformal mappings. Hence, if we take u as the form (2.2), then u is a CGO solution to (1.2) in Ω_0 . We want to remark that L is a nonzero vector satisfying a Cauchy–Riemann type equation. Denote $L = \begin{pmatrix} \ell \\ d \end{pmatrix}$ with $\ell \in \mathbb{C}^2$ and $d \in \mathbb{C}^1$. Generically, we can assume that both ℓ and d do not vanish in Ω_0 (see [19, Remarks 3.1 and 4.1]).

Due to the conformality of ρ, φ and ψ are harmonic functions in Ω_0 . Conversely, given any φ harmonic in Ω_0 with $\nabla\varphi \neq 0$ in Ω_0 , we can find a harmonic conjugate ψ of φ in Ω_0 so that $\rho = \varphi + i\psi$ is conformal in Ω_0 . The freedom of choosing φ plays a key role in our reconstruction method for the object identification problem. Actually, we will mainly focus on level curves of φ . As in [20], we choose $\rho(x)$ to be complex polynomials.

Pick a point $x_0 \notin \overline{\Omega}$. It is no restriction to assume $x_0 = 0$. We now consider $\varphi_N = \text{Re}(c_N x^N)$ for $N \geq 2$, where $c_N \in \mathbb{C}$ with $|c_N| = 1$. In the polar coordinates, $\varphi_N(r, \theta) = r^N \cos N(\theta - \theta_N)$ for some θ_N determined by c_N . We observe that $\varphi_N > 0$ in some open cone Γ_N with an opening angle π/N . Now assume that $\Gamma_N \cap \Omega \neq \emptyset$. The complex function $\rho_N(x) = c_N x^N = \varphi_N + i\psi_N$ is clearly conformal in Ω . For solving the inverse problem, we want to shrink the opening angle of Γ_N by taking $N \rightarrow \infty$. However, there are two serious problems in doing so. On one hand, φ_N is periodic in the angular variable, which means that it is positive in some other cones with the same opening angle which also intersect Ω when N is large. This property of φ_N prohibits us from using corresponding CGO solutions with large N to the object identification problem. On the other hand, the complex function $\rho_N(x)$ fails to be injective in the whole domain Ω when N is large. To overcome those difficulties and construct useful CGO solutions in the whole domain Ω , we shall carry out the construction described above in

$$\Omega_0 = \Gamma_N \cap \Omega,$$

and extend the constructed solutions to Ω by cut-off functions. From now on, we assume that Ω_0 is bounded.

We first note that ρ_N is conformal in Ω_0 and is bijective from Ω_0 onto $\rho_N(\Omega_0)$. We denote:

$$U_{N,h}(x) = \begin{pmatrix} w_{N,h} \\ g_{N,h} \end{pmatrix} = e^{(\varphi_N + i\psi_N)/h} (L + R),$$

solving (2.1) in Ω_0 . That is,

$$u_{N,h} = \mu^{-1/2} w_{N,h} + \mu^{-1} \nabla g_{N,h} - g_{N,h} \nabla \mu^{-1},$$

satisfies (1.2) in Ω_0 . Now to get solutions of (1.2) in the whole domain Ω , we use a cut-off technique. For $s > 0$, let $l_s = \{x \in \Gamma_N : \varphi_N = s^{-1}\}$. This is the level curve of φ_N in Γ_N . Let $0 < t < t_0$ such that

$$\left(\bigcup_{s \in (0,t)} l_s \right) \cap \Omega \neq \emptyset,$$

and choose a small $\varepsilon > 0$. Define a cut-off function $\phi_{N,t}(x) \in C^\infty(\mathbb{R}^2)$ so that $\phi_{N,t}(x) = 1$ for $x \in \overline{\bigcup_{s \in (0,t+\varepsilon/2)} l_s} \cap \Omega$ and is zero for $x \in \overline{\Omega} \setminus (\bigcup_{s \in (0,t+\varepsilon)} l_s)$. We now define:

$$u_{N,t,h}(x) = \phi_{N,t} e^{-t^{-1}/h} u_{N,h},$$

for $x \in (\bigcup_{s \in (0,t+\varepsilon)} l_s) \cap \Omega$. So $u_{N,t,h}$ can be regarded as a function in Ω which is zero outside of Ω_0 . We now take $f_{N,t,h} = u_{N,t,h}|_{\partial\Omega}$. We remark that $f_{N,t,h}$ can be used as the boundary data in the inverse problem. An obvious reason of using $f_{N,t,h}$ is that they are local and so we only need to collect Neumann data over the support of $f_{N,t,h}$ when we

study the object identification problem with boundary measurements. Note that since Ω_0 is bounded, we can see that $u_{N,t,h} \in H^1(\Omega)$ and therefore

$$f_{N,t,h} \in H^{1/2}(\partial\Omega).$$

The function $u_{N,t,h}$ is not a solution to the elasticity equation in Ω . However, we shall show that the difference between $u_{N,t,h}$ and the true solution to the elasticity equation with the same Dirichlet condition as $u_{N,t,h}$ is exponentially small. Precisely, let us consider the boundary value problem:

$$\begin{cases} \mathcal{L}w_{N,t,h} = 0 & \text{in } \Omega, \\ w_{N,t,h} = f_{N,t,h} & \text{on } \partial\Omega. \end{cases} \tag{2.6}$$

Then we can show that

Lemma 2.1. *There exists a unique solution $w_{N,t,h}$ to (2.6). Moreover, there exist $C > 0$ and $\varepsilon' > 0$ such that*

$$\|u_{N,t,h} - w_{N,t,h}\|_{H^1(\Omega)} \leq C e^{-\varepsilon'/h}. \tag{2.7}$$

Proof. Denote $\tilde{u}_{N,t,h} = u_{N,t,h} - w_{N,t,h}$. Then $\tilde{u}_{N,t,h}$ satisfies:

$$\begin{cases} \mathcal{L}\tilde{u}_{N,t,h} = g_{N,t,h} & \text{in } \Omega, \\ \tilde{u}_{N,t,h} = 0 & \text{on } \partial\Omega, \end{cases}$$

where $g_{N,t,h} = \mathcal{L}u_{N,t,h}$. Note that $\mathcal{L}u_{N,t,h} = 0$ in $(\bigcup_{s \in (0,t_0)} I_s) \cap \Omega$ and $\partial_{x_j} \phi_{N,t}(x)$ for $j = 1, 2$ are supported in

$$\overline{\left(\bigcup_{s \in (t+\varepsilon/2, t+\varepsilon)} I_s \right) \cap \Omega}.$$

So $g_{N,t,h}$ is supported in $\overline{(\bigcup_{s \in (t+\varepsilon/2, t+\varepsilon)} I_s) \cap \Omega}$ and we have that

$$\|g_{N,t,h}\|_{L^2(\Omega)} \leq C' e^{-\varepsilon'/h} \tag{2.8}$$

for some $C' > 0$ and $\varepsilon' > 0$. Now the lemma follows from the first Korn inequality and the Lax–Milgram theorem. \square

3. Reconstruction of inclusions

We will use the special solutions constructed in the previous section to study the inverse problem of reconstructing embedded inclusions. Here we follow the presentation given in [19]. Assume that Ω is either a bounded domain or an infinite strip. Also, let $0 \notin \overline{\Omega}$ and $\Omega = \{(x_1, x_2) : x_1 \in \mathbb{R}, a < x_2 < b < 0\}$ if Ω is a strip. Now consider D an open subset of Ω with Lipschitz boundary satisfying that $D \Subset \Omega$ and $\Omega \setminus \overline{D}$ is connected. Suppose that $\lambda_0(x) \in C^2(\overline{\Omega})$ and $\mu_0(x) \in C^4(\overline{\Omega})$ satisfy the strong convexity condition, i.e.,

$$\lambda_0(x) + \mu_0(x) > 0 \quad \text{and} \quad \mu_0(x) > 0 \quad \forall x \in \overline{\Omega}. \tag{3.1}$$

It is obvious that (3.1) implies (1.1). On the other hand, we assume that $\tilde{\lambda}(x), \tilde{\mu}(x)$ be two essentially bounded functions such that either

$$\tilde{\mu} \geq 0 \quad \text{and} \quad \tilde{\lambda} + \tilde{\mu} \geq 0 \quad \text{a.e. in } D,$$

or

$$\tilde{\mu} \leq 0 \quad \text{and} \quad \tilde{\lambda} + \tilde{\mu} \leq 0 \quad \text{a.e. in } D.$$

Furthermore, suppose that $\lambda = \lambda_0 + \chi_D \tilde{\lambda}$ and $\mu = \mu_0 + \chi_D \tilde{\mu}$ satisfy (3.1) a.e. in Ω , where χ_D is the characteristic function of D . Therefore, for any $f \in H^{1/2}(\partial\Omega)$, there exists a unique (weak) solution u to,

$$\begin{cases} \mathcal{L}_D u = 0 & \text{in } \Omega, \\ u = f & \text{on } \partial\Omega. \end{cases} \tag{3.2}$$

Here the elastic operator \mathcal{L}_D is defined in terms of λ and μ . As before, we can prove the well-posedness of (3.2) by combining the first Korn inequality and the Lax–Milgram theorem. The arguments remain valid even when Ω is an infinite strip. The Dirichlet-to-Neumann map related to \mathcal{L}_D is now defined as

$$\Lambda_D : f \rightarrow \sigma(u)\mathbf{n}|_{\partial\Omega},$$

where \mathbf{n} is the unit outer normal of $\partial\Omega$ and for $x \in \partial\Omega$,

$$\sigma(u) = \lambda(\nabla \cdot u)I + 2\mu S(\nabla u) = \lambda_0(\nabla \cdot u)I + 2\mu_0 S(\nabla u).$$

Now assume that all parameters are known except $\tilde{\lambda}$, $\tilde{\mu}$, and D . The inverse problem is to determine D by Λ_D . Here we will provide a reconstruction algorithm to this inverse problem. We begin with some useful integral inequalities. Let Λ_0 be the Dirichlet-to-Neumann map related to \mathcal{L}_0 , where \mathcal{L}_0 is the elastic operator defined in terms of λ_0 and μ_0 . Assume that u_0 is the solution of

$$\begin{cases} \mathcal{L}_0 u_0 = 0 & \text{in } \Omega, \\ u_0 = f & \text{on } \partial\Omega. \end{cases} \tag{3.3}$$

Then one can derive the following integral inequalities:

Lemma 3.1.

$$\begin{aligned} & \int_D \left\{ \frac{\lambda_0 + \mu_0}{\lambda + \mu} (\tilde{\lambda} + \tilde{\mu}) |\nabla \cdot u_0|^2 + 2 \frac{\mu_0}{\mu} \tilde{\mu} \left| S(\nabla u_0) - \frac{\nabla \cdot u_0}{2} I_2 \right|^2 \right\} dx \\ & \leq \langle (\Lambda_D - \Lambda_0) f, \bar{f} \rangle \\ & \leq \int_D \left\{ (\tilde{\lambda} + \tilde{\mu}) |\nabla \cdot u_0|^2 + 2 \tilde{\mu} \left| S(\nabla u_0) - \frac{\nabla \cdot u_0}{2} I_2 \right|^2 \right\} dx. \end{aligned} \tag{3.4}$$

Proof. Similar inequalities for the three-dimensional isotropic elasticity were given in [8, Proposition 5.1]. One can prove (3.4) using some identities in [7] (see (3.8), (3.9) in [7]). Here we give a direct proof following the arguments in [8]. By virtue of the definition of the Dirichlet-to-Neumann map, we can see that

$$\begin{aligned} \langle (\Lambda_0 - \Lambda_D) f, \bar{f} \rangle &= \int_{\Omega} \left\{ \lambda |\nabla \cdot (u - u_0)|^2 + 2\mu |S(\nabla u) - S(\nabla u_0)|^2 \right. \\ & \quad \left. + (\lambda_0 - \lambda) |\nabla \cdot u_0|^2 + 2(\mu_0 - \mu) |S(\nabla u_0)|^2 \right\} dx. \end{aligned} \tag{3.5}$$

We now write:

$$S(\nabla u_0) = \left(S(\nabla u_0) - \frac{\nabla \cdot u_0}{2} I_2 \right) + \frac{\nabla \cdot u_0}{2} I_2 = T_0 + \frac{\nabla \cdot u_0}{2} I_2,$$

and

$$S(\nabla u) = \left(S(\nabla u) - \frac{\nabla \cdot u}{2} I_2 \right) + \frac{\nabla \cdot u}{2} I_2 = T + \frac{\nabla \cdot u}{2} I_2.$$

Note that the traces of T_0 and T vanish. Thus $T_0 \cdot I_2 = T \cdot I_2 = 0$. Therefore, we have that

$$|S(\nabla u_0)|^2 = |T_0|^2 + \frac{1}{2} |\nabla u_0|^2, \quad |S(\nabla u)|^2 = |T|^2 + \frac{1}{2} |\nabla u|^2,$$

and (3.5) becomes:

$$\begin{aligned} \langle (\Lambda_0 - \Lambda_D) f, \bar{f} \rangle &= \int_{\Omega} \left\{ (\lambda + \mu) |\nabla \cdot (u - u_0)|^2 + 2\mu |T - T_0|^2 \right. \\ & \quad \left. + ((\lambda_0 - \lambda) + (\mu_0 - \mu)) |\nabla \cdot u_0|^2 + 2(\mu_0 - \mu) |T_0|^2 \right\} dx. \end{aligned} \tag{3.6}$$

Since $\lambda + \mu > 0$ and $\mu > 0$, the second inequality of (3.4) follows from (3.6) immediately.

Exchanging the roles of u and u_0 , (3.6) changes to

$$\begin{aligned} \langle (\Lambda_D - \Lambda_0)f, \bar{f} \rangle &= \int_{\Omega} \left\{ (\lambda_0 + \mu_0)|\nabla \cdot (u_0 - u)|^2 + 2\mu_0|T_0 - T|^2 \right. \\ &\quad \left. + ((\lambda - \lambda_0) + (\mu - \mu_0))|\nabla \cdot u|^2 + 2(\mu - \mu_0)|T|^2 \right\} dx. \end{aligned} \tag{3.7}$$

Next we estimate the integrand on the right-hand side of (3.7). We compute:

$$\begin{aligned} &(\lambda_0 + \mu_0)|\nabla \cdot (u_0 - u)|^2 + 2\mu_0|T_0 - T|^2 + ((\lambda - \lambda_0) + (\mu - \mu_0))|\nabla \cdot u|^2 + 2(\mu - \mu_0)|T|^2 \\ &= (\lambda_0 + \mu_0)|\nabla \cdot u_0|^2 - (\lambda_0 + \mu_0)\nabla \cdot u \nabla \cdot \bar{u}_0 - (\lambda_0 + \mu_0)\nabla \cdot \bar{u} \nabla \cdot u_0 + (\lambda + \mu)|\nabla \cdot u|^2 + 2\mu_0|T_0|^2 \\ &\quad - 2\mu_0 T \cdot \bar{T}_0 - 2\mu_0 \bar{T} \cdot T_0 + 2\mu|T|^2 \\ &= \left| \sqrt{\lambda + \mu} \nabla \cdot u - \frac{\lambda_0 + \mu_0}{\sqrt{\lambda + \mu}} \nabla \cdot u_0 \right|^2 + \left| \sqrt{2\mu} T - \frac{2\mu_0}{\sqrt{2\mu}} T_0 \right|^2 + \frac{\lambda_0 + \mu_0}{\lambda + \mu} [(\lambda - \lambda_0) + (\mu - \mu_0)] |\nabla \cdot u_0|^2 \\ &\quad + 2 \frac{\mu_0}{\mu} (\mu - \mu_0) |T_0|^2. \end{aligned} \tag{3.8}$$

Combining (3.7) and (3.8), we have the first inequality of (3.4). \square

We are now at a position to discuss the inverse problem. First of all, we give an appropriate jump condition across ∂D :

for $y \in \partial D$, there exists a ball $B_\epsilon(y)$ such that *one* of the following conditions holds:

$$\begin{cases} \tilde{\mu} > \epsilon, \tilde{\lambda} + \tilde{\mu} \geq 0, \\ \tilde{\mu} = 0, \tilde{\lambda} > \epsilon, \\ \tilde{\mu} < -\epsilon, \tilde{\lambda} + \tilde{\mu} \leq 0, \\ \tilde{\mu} = 0, \tilde{\lambda} < -\epsilon. \end{cases} \quad \forall x \in B_\epsilon(y) \cap D, \tag{3.9}$$

Now let $w_{N,t,h}$ be the solution of (3.3) with the Dirichlet condition $f = f_{N,t,h}$. To construct the inclusion D , we rely on the quantity:

$$E(N, t, h) = \langle (\Lambda_D - \Lambda_0)f_{N,t,h}, \bar{f}_{N,t,h} \rangle.$$

Clearly, this quantity is completely determined by the boundary data localized in $\Gamma_N \cap \partial\Omega$. This localization property is of great value in actual applications, especially when Ω is an infinite strip. Now $E(N, t, h)$ satisfies the integral inequality (3.4) with u_0 being replaced by $w_{N,t,h}$, i.e.

$$\begin{aligned} &\int_D \left\{ \frac{\lambda_0 + \mu_0}{\lambda + \mu} (\tilde{\lambda} + \tilde{\mu}) |\nabla \cdot w_{N,t,h}|^2 + 2 \frac{\mu_0}{\mu} \tilde{\mu} \left| S(\nabla w_{N,t,h}) - \frac{\nabla \cdot w_{N,t,h}}{2} I_2 \right|^2 \right\} dx \\ &\leq E(N, t, h) \\ &\leq \int_D \left\{ (\tilde{\lambda} + \tilde{\mu}) |\nabla \cdot w_{N,t,h}|^2 + 2\tilde{\mu} \left| S(\nabla w_{N,t,h}) - \frac{\nabla \cdot w_{N,t,h}}{2} I_2 \right|^2 \right\} dx. \end{aligned} \tag{3.10}$$

Argued as in [19] and [20], we can prove the following important behaviors of $E(N, t, h)$.

Theorem 3.2. *Let $t > 0$ and $\mathcal{D}_t = \{x \in \Gamma_N : \varphi_N \geq t^{-1}\}$. Assume that one of the jump conditions (3.9) holds. Then we have:*

- (i) *if $\mathcal{D}_t \cap \bar{D} = \emptyset$ then there exist $C_1 > 0$, $\epsilon_1 > 0$, and $h_1 > 0$ such that $E(N, t, h) \leq C_1 e^{-\epsilon_1/h}$ for all $h \leq h_1$;*
- (ii) *if $\mathcal{D}_t \cap D \neq \emptyset$ then there exist $C_2 > 0$, $\epsilon_2 > 0$, and $h_2 > 0$ such that $E(N, t, h) \geq C_2 e^{\epsilon_2/h}$ for all $h \leq h_2$.*

Proof. The proof here relies on the integral inequalities (3.10). Replacing $w_{N,t,h}$ in (3.10) by $u_{N,t,h}$ and taking into account of (2.7) leads to

$$\begin{aligned} & \int_D \left\{ \frac{\lambda_0 + \mu_0}{\lambda + \mu} (\tilde{\lambda} + \tilde{\mu}) |\nabla \cdot u_{N,t,h}|^2 + 2 \frac{\mu_0}{\mu} \tilde{\mu} \left| S(\nabla u_{N,t,h}) - \frac{\nabla \cdot u_{N,t,h}}{2} I_2 \right|^2 \right\} dx + O(e^{-\varepsilon'/h}) \\ & \leq E(N, t, h) \\ & \leq \int_D \left\{ (\tilde{\lambda} + \tilde{\mu}) |\nabla \cdot u_{N,t,h}|^2 + 2\tilde{\mu} \left| S(\nabla u_{N,t,h}) - \frac{\nabla \cdot u_{N,t,h}}{2} I_2 \right|^2 \right\} dx + O(e^{-\varepsilon'/h}). \end{aligned} \tag{3.11}$$

Recall that

$$u_{N,t,h}(x) = \phi_{N,t} e^{-t^{-1}/h} u_{N,h} = \phi_{N,t} e^{-t^{-1}/h} \{ \mu_0^{-1/2} w_{N,h} + \mu_0^{-1} \nabla g_{N,h} - g_{N,h} \nabla \mu_0^{-1} \},$$

where $\begin{pmatrix} w_{N,h} \\ g_{N,h} \end{pmatrix}$ solves (2.1) in Ω with Lamé parameters λ_0 and μ_0 . We now write:

$$w_{N,h} = e^{(\varphi_N + i\psi_N)/h} (\ell + r) \quad \text{and} \quad g_{N,h} = e^{(\varphi_N + i\psi_N)/h} (d + s).$$

Through tedious but straightforward computations, the leading terms of $\nabla \cdot u_{N,t,h}$ and $S(\nabla u_{N,t,h})$ are respectively,

$$e^{(\varphi_N - t^{-1} + i\psi_N)/h} \mu_0^{-1/2} \left(1 - \frac{\lambda_0 + \mu_0}{\lambda_0 + 2\mu_0} \right) \frac{\nabla \varphi_N + i \nabla \psi_N}{h} \cdot \ell,$$

and

$$e^{(\varphi_N - t^{-1} + i\psi_N)/h} \mu_0^{-1} \frac{1}{h^2} \nabla(\varphi + i\psi) \otimes \nabla(\varphi + i\psi) d$$

(see [19]).

Assume that the first assumption of (3.9) holds. Then the leading terms of two integrals in (3.11) come from $S(\nabla u_{N,t,h})$ and are determined by:

$$\frac{1}{h^4} e^{2(\varphi_N - t^{-1})/h} ((\nabla \varphi_N)^2 + (\nabla \psi_N)^2)^2 |d|^2. \tag{3.12}$$

On the other hand, if the second assumption of (3.9) holds, then the leading terms in those integrals in (3.11) come from $\nabla \cdot u_{N,t,h}$ and are governed by:

$$\frac{2}{h^2} e^{2(\varphi_N - t^{-1})/h} (\nabla \varphi_N)^2 |\ell|^2. \tag{3.13}$$

Now the statement (i) and (ii) follow directly from (3.11) and (3.12) or (3.13). The other two cases of (3.9) are treated similarly. \square

In view of Theorem 3.2, we are able to reconstruct some part of ∂D by looking into the asymptotic behavior of $E(N, t, h)$ for various t 's. More precisely, let:

$$t_{D,N} := \sup \left\{ t \in (0, \infty) : \lim_{h \rightarrow 0} E(N, h, t) = 0 \right\},$$

then if $t_{D,N} = \infty$ we have $\Gamma_N \cap D = \emptyset$. On the other hand, if $t_{D,N} < \infty$ then there exists a $p_{D,N} \in \mathcal{D}_{t_{D,N}} \cap \partial D$.

By taking N arbitrarily large (the opening angle of Γ_N becomes arbitrarily small), we can reconstruct even more information of ∂D . A point p on ∂D is said to be *detectable* if there exists a semi-straight line L starting from p such that L does not intersect ∂D except p . For example, if D is star-shaped, every point of ∂D is detectable.

Corollary 3.3. *Every detectable point of ∂D can be reconstructed from Λ_D .*

We refer to [20] for a proof of this corollary. To end this section, we give an algorithm of our reconstruction method.

Step 1. Pick a point $x_0 \notin \bar{\Omega}$ (but close to $\bar{\Omega}$). Given $N \in \mathbb{N}$ and choose the cone Γ_N which intersects Ω .

- Step 2. Start with $t > 0$ such that $\mathcal{D}_t \cap \Omega \neq \emptyset$. Construct $u_{N,t,h}$ and determine the Dirichlet data $f_{N,t,h} = u_{N,t,h}|_{\partial\Omega}$.
- Step 3. Compute $E(N, t, h) = \int_{\text{supp}(f_{N,t,h})} (\Lambda_D - \Lambda_0) f_{N,t,h} \cdot \bar{f}_{N,t,h} ds$.
- Step 4. If $E(N, t, h)$ is arbitrarily small, then increase t and repeat Steps 2 and 3; if $E(N, t, h)$ is arbitrarily large, then decrease t and repeat Steps 2 and 3.
- Step 5. Repeat Step 4 to get a good approximation of ∂D in Γ_N .
- Step 6. Move the cone Γ_N around x_0 by taking a different c_N in $\varphi_N = \text{Re}(c_N x^N)$. Repeat Steps 2–5.
- Step 7. Choose a larger N and a new cone Γ_N . Repeat Steps 2–6.
- Step 8. Pick a different x_0 and repeat Steps 1–7.

4. Numerical results

4.1. Preliminaries

In this section, we provide some computational results based on our method. We shall demonstrate numerical results for two cases – Ω is a rectangle and Ω is an infinite strip. In both cases, we assume that the background parameters λ_0, μ_0 satisfy $\lambda_0(x) \equiv \lambda > 0$ and $\mu_0(x) \equiv \mu > 0$ for all $x \in \Omega$. For such λ_0 and μ_0 , we can construct special solutions $u_{N,h}$ satisfying $\mathcal{L}_0 u_{N,h} = 0$ quite explicitly. In other words, we do not need to go through the general procedures given in Section 2. More precisely, for λ_0, μ_0 given here, the corresponding matrices A and Q in (2.1) are reduced to

$$A(x) = \begin{pmatrix} 0 & 0 \\ 0 & \zeta \end{pmatrix},$$

and

$$Q(x) \equiv 0,$$

where $\zeta = \frac{\lambda+\mu}{\lambda+2\mu} \mu^{1/2} > 0$. Therefore, (2.1) can be written as

$$\begin{cases} \Delta w = 0, \\ \Delta g + \zeta \nabla \cdot w = 0. \end{cases} \tag{4.1}$$

To construct special solutions for (4.1), we first choose,

$$w = e^{(\varphi+i\psi)/h} w_0,$$

where $w_0 = \nabla\varphi + i\nabla\psi$. To simplify the notations, we denote $\varphi = \varphi_N$ and $\psi = \psi_N$. To check that w satisfies the first equation of (4.1), we note that

$$\Delta\varphi + i\Delta\psi = 0 \quad \text{and} \quad (\nabla\varphi + i\nabla\psi)^2 = 0. \tag{4.2}$$

Therefore, from (4.2) we obtain:

$$\begin{aligned} \Delta w &= \Delta(e^{(\varphi+i\psi)/h} w_0) \\ &= \Delta e^{(\varphi+i\psi)/h} w_0 + 2\nabla(e^{(\varphi+i\psi)/h}) \cdot \nabla w_0 + e^{(\varphi+i\psi)/h} \Delta w_0 \\ &= \frac{2}{h} e^{(\varphi+i\psi)/h} (\nabla\varphi + i\nabla\psi) \cdot \nabla w_0 + e^{(\varphi+i\psi)/h} \nabla(\Delta\varphi + i\Delta\psi) \\ &= \frac{1}{h} e^{(\varphi+i\psi)/h} \nabla(\nabla\varphi + i\nabla\psi)^2 \\ &= 0. \end{aligned}$$

Furthermore, due to (4.2), we observe that

$$\nabla \cdot w = 0.$$

Thus, we simply choose $g \equiv 0$ and the second equation of (4.1) holds. In other words,

$$u_{N,h} = e^{(\varphi_N+i\psi_N)/h} (\nabla\varphi_N + i\nabla\psi_N),$$

satisfies $\mathcal{L}_0 u_{N,h} = 0$. Thus, our simulated (exact) Dirichlet condition is given by:

$$f_{N,t,h} = \phi_{N,t} e^{-t^{-1}/h} e^{(\varphi_N + i\psi_N)/h} (\nabla \varphi_N + i \nabla \psi_N)|_{\partial\Omega}.$$

To indicate the dependence of φ_N and ψ_N on the vertex point of the associated cone, in what follows, we will write $\varphi_N = \varphi_N(x, x_0)$ and $\psi_N = \psi_N(x, x_0)$, where x_0 stands for the vertex point.

We now describe our reconstruction strategies. The same procedures were also used in [6] and [20]. In our program, in order to show the numerical results more efficiently without using excessive computational time, we fix $N = 4$ and probe the region Ω by moving the vertex point of the probing cone with $\theta_4 = 0$ (i.e., without rotating the probing cone). Hence, we first design M different probing cones based on M different vertex points. Remind that each cone is congruent to the cone with vertex at the origin and opening angle $\pi/4$. We then take appropriate h_1 and h_2 with $h_1 > h_2$ and choose a suitable number of probing fronts determined by t_j for $j = 1, \dots, J$ with $t_j < t_{j+1}$. In each probing cone Γ_m ($m = 1, \dots, M$) given above, we construct the Dirichlet data f supported in the intersection of Γ_m and the bottom boundary of $\partial\Omega$ for every h_k and t_j , $k = 1, 2$, $j = 1, \dots, J$. We now evaluate $E_{j,k} := E(N, t_j, h_k)$ and determine t_n such that

$$E_{n+1,2} > E_{n+1,1}. \tag{4.3}$$

Then the region R_m defined by:

$$R_m = \{x \in \Gamma_m : \varphi_N(x, x_0) \leq t_n^{-1}\},$$

is the estimated largest region in Γ_m which does not contain the inclusion. So the region $R := \bigcup_{m=1}^M R_m$ is the estimated largest region with absence of inclusion with a given sweeping scheme. We would like to point out that condition (4.3) is our rule of thumb in determining whether the level curve $\varphi_N(x, x_0) = t^{-1}$ intersects the inclusion in our numerical experiments. It is not equivalent to Theorem 3.2, but based on the reasoning that $E(N, t, h)$ is exponentially decaying when $\varphi_N(x, x_0) = t^{-1}$ stays away from the inclusion and exponentially growing when $\varphi_N(x, x_0) = t^{-1}$ intersects the inclusion.

To show the effect of noise to our method, we add appropriate noise to the simulated data. We consider the form of noise given in [6]. To be precise, let $\eta : [-1, 1] \mapsto \mathbb{C}$ be a random function defined by:

$$\eta(s) = \sum_{k=-32}^{32} (a_k + i b_k) e^{iks\pi/2},$$

where $a_k, b_k \sim \mathcal{N}(0, 1)$ are normally distributed random numbers. For the conductivity problem, the number 32 in η is chosen to roughly model a collection of 32 electrodes on the bottom boundary of Ω . Measurement noise is modeled by $\Lambda_D f$ by $\Lambda_D f + c\eta$ with

$$c = \frac{A \|\Lambda_D f\|_\infty}{\|\eta\|_\infty},$$

where $A > 0$. Finally, we would like to point out that in our simulation, a big chunk of computational time is used to obtain the simulated data. This is the forward problem. Once having the simulated data, the inverse procedure is rather trivial. In order to obtain desired accuracy on the simulated data and be able to adapt to different shapes of inclusions, we use the finite element method (FEM) to solve the forward problem. In our FEM program, we perform the grid refinement near the boundary and the inclusion to ensure the accuracy of the simulated data (see Fig. 1 for example).

4.2. Ω is a rectangle

In our numerical computations, we take the domain:

$$\Omega = \{(x_1, x_2) : -1 < x_1 < 1, -1.01 < x_2 < -0.01\}.$$

We shall use the Dirichlet data localized on $\{(x_1, -0.01) : -1 < x < 1\}$ (top boundary), $\{(x_1, -1.01) : -1 < x < 1\}$ (bottom boundary). To this end, we choose vertex points from $\{x_2 = -1.02\}$ and $\{x_2 = 0\}$, respectively. Let $x_0 = (x_{0,1}, x_{0,2})$ denote the vertex point and we write

$$\rho_4(x, x_0) := \varphi_4(x, x_0) + i\psi_4(x, x_0) = ((x_1 - x_{0,1}) + i(x_2 - x_{0,2}))^4.$$

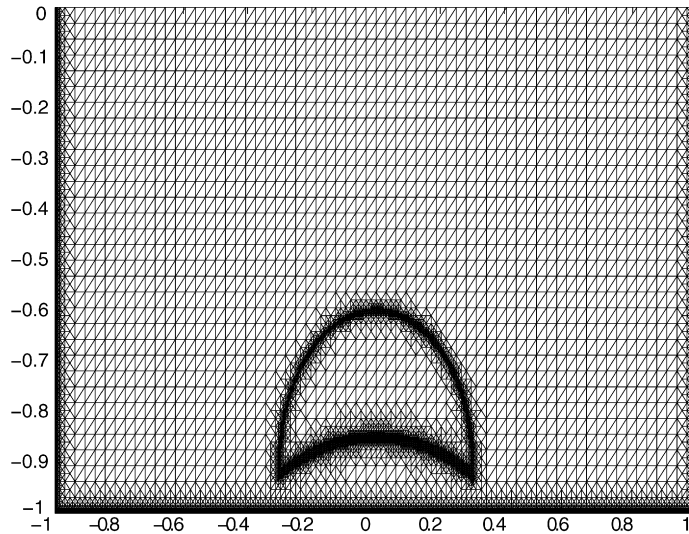


Fig. 1. Example of our FEM meshes.

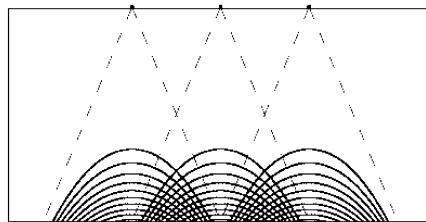


Fig. 2. Probing fronts of our numerical method. In this figure, the nonzero Dirichlet condition is on the bottom boundary.

Thus, the probing fronts are level curves of φ_4 . In Fig. 2, we show some probing fronts with nonzero Dirichlet condition on the bottom. To set up the Dirichlet condition, we ignore the cut-off function $\phi_{N,t}$ and take:

$$f_{N,t,h}|_{\partial\Omega} = \begin{cases} e^{(\rho_4(x,x_0)-t^{-1})/h} \nabla \rho_4(x, x_0), & \text{for } (x_1, x_2) \in \partial\Omega_{\text{obs}}, \\ 0, & \partial\Omega \setminus \partial\Omega_{\text{obs}}, \end{cases}$$

where $\partial\Omega_{\text{obs}}$ is determined by x_0 . For example, if $x_0 = (0, 0)$, then

$$\partial\Omega_{\text{obs}} = \left\{ (x_1, x_2): -1.01 \times \tan\left(\frac{\pi}{8}\right) < x_1 < 1.01 \times \tan\left(\frac{\pi}{8}\right), x_2 = -1.01 \right\}.$$

In the following figures, we show our reconstruction method for three cases with different inclusions. As we mentioned above, due to computational costs, we only provide numerical results obtained by putting nonzero Dirichlet condition on either the top or the bottom boundaries. In conventional expression, we describe the elastic medium by the Young’s modulus E and the Poisson ratio ν . The relation between (E, ν) and (λ, μ) is given by:

$$\lambda = \frac{E\nu}{1-\nu^2} \quad \text{and} \quad \mu = \frac{E}{2(1+\nu)}.$$

In our simulations, we take $(E, \nu) = (6 \times 10^6, 0.45)$ for the background medium (gray area) and $(E, \nu) = (6 \times 10^7, 0.45)$ inside of the inclusions (black area) (see Fig. 3).

We now want to make some remarks on the figures mentioned above. Since we are only probing the region from the top and the bottom boundaries, we are unable to resolve the inclusion-free near the left and the right boundaries. Thus, the area on near those boundaries are black. Moving the nonzero Dirichlet condition $f_{N,t,h}$ to those places will certainly improve the resolution of the inclusion. But we need to pay the price of at least double the computational cost. We believe that showing the figures obtained by probing from the top and the bottom is sufficient to demonstrate the essential ideas of our method.

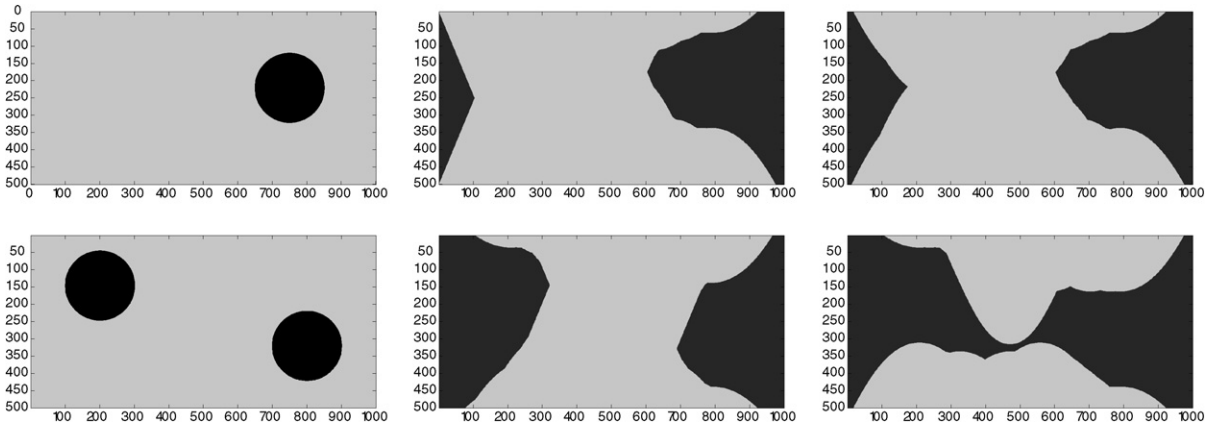


Fig. 3. The first column represents the actual location of the inclusion. The second column is the numerical reconstruction with noiseless simulated data. The third column is the numerical reconstruction with noisy data with $A = 0.01\%$. All gray areas are inclusion-free regions.

4.3. Ω is a strip

Here we assume $\Omega = \{(x_1, x_2): -\infty < x_1 < \infty, -1.01 < x_2 < -0.01\}$. In order to get the simulated data in this case, we need to impose appropriate artificial boundary conditions in the x_1 direction. We now rewrite elasticity system (1.2) or (1.3) into,

$$\begin{pmatrix} \lambda + 2\mu & 0 \\ 0 & \mu \end{pmatrix} \partial_1^2 u + \begin{pmatrix} 0 & \lambda + \mu \\ \lambda + \mu & 0 \end{pmatrix} \partial_1 \partial_2 u + \begin{pmatrix} \mu & 0 \\ 0 & \lambda + 2\mu \end{pmatrix} \partial_2^2 u = 0. \tag{4.4}$$

The characteristic polynomial related to (4.4) is:

$$P(\xi) := \begin{pmatrix} \lambda + 2\mu & 0 \\ 0 & \mu \end{pmatrix} \xi_1^2 + \begin{pmatrix} 0 & \lambda + \mu \\ \lambda + \mu & 0 \end{pmatrix} \xi_1 \xi_2 + \begin{pmatrix} \mu & 0 \\ 0 & \lambda + 2\mu \end{pmatrix} \xi_2^2,$$

which is a symmetric quadratic matrix polynomial. Motivated by the factorizations of symmetric quadratic matrix polynomials, by some computations, we can see that

$$P(\xi) = (I\xi_1 - B^T \xi_2) \begin{pmatrix} \lambda + 2\mu & 0 \\ 0 & \mu \end{pmatrix} (I\xi_1 - B\xi_2),$$

with

$$B = \begin{pmatrix} 0 & -1 \\ 1 & 0 \end{pmatrix}.$$

Therefore, system (4.4) can be factored into

$$(I\partial_1 - B^T \partial_2) \begin{pmatrix} \lambda + 2\mu & 0 \\ 0 & \mu \end{pmatrix} (I\partial_1 - B\partial_2)u = 0. \tag{4.5}$$

In view of (4.5), on any artificial boundary $x_1 = a$, we impose condition

$$\partial_1 u(a, x_2) - B\partial_2 u(a, x_2) = 0. \tag{4.6}$$

Explicitly, in our numerical simulation, we truncate the infinite strip Ω into a rectangle considered in Section 4.2. For example, in case of $x_0 = (0, 0)$, we impose the boundary condition as follows:

$$\begin{cases} u = e^{(\rho_4(x, x_0) - t^{-1})/h} \nabla \rho_4(x, x_0) & (x_1, x_2) \text{ in } \partial\Omega_{\text{obs}}, \\ \partial_1 u(1, x_2) = B\partial_2 u(1, x_2) & \text{for } -0.01 < x_2 < -1.01, \\ \partial_1 u(-1, x_2) = B\partial_2 u(-1, x_2) & \text{for } -0.01 < x_2 < -1.01, \\ u = 0 & \text{elsewhere.} \end{cases} \tag{4.7}$$

We will indicate how to implement boundary condition (4.7) in the FEM method in Appendix A. The computational results for the strip case with noiseless and noisy data are given in Fig. 4.

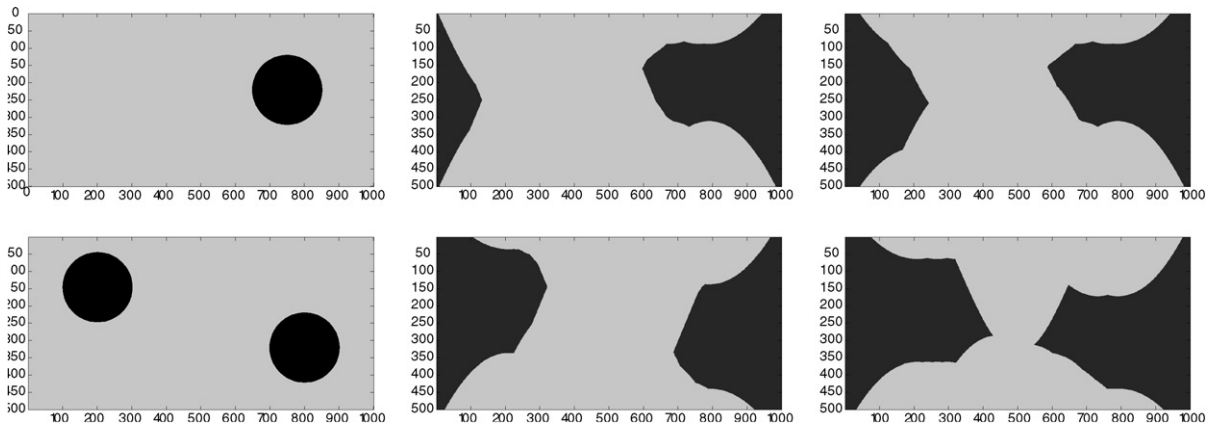


Fig. 4. The first column represents the actual location of inclusions. The second column is the numerical reconstruction with noiseless simulated data. The third column is the numerical reconstruction with noisy data with $A = 0.01\%$. All gray areas are inclusion-free regions.

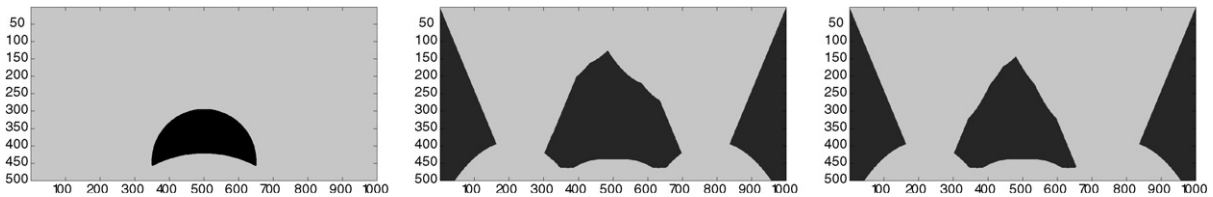


Fig. 5. The first column is the actual location of the inclusion. The second column is the numerical reconstruction with noiseless simulated data when Ω is a rectangle. The third column is the numerical reconstruction with noiseless simulated data when Ω is a strip. All gray areas are inclusion-free regions.

4.4. Ill-posedness

Supported by numerical evidence, it is widely believed that when the unknown object is far away from the boundary, the determination problem by boundary measurements is more ill-posed than the case where the object is near the boundary. The following figures give further examples of this interesting phenomenon. In Fig. 5, we can see that the lower part of the inclusion is clearly resolved; while, the upper part of the inclusion is difficult to detect.

5. Conclusions

In this article, we present a numerically feasible reconstruction algorithm for the determination of inclusions by boundary measurements for the two-dimensional isotropic elasticity system. The domain can also be unbounded. We point out that the same method works for the cavity case. Our method depends on a new type of CGO solutions for the elasticity system. Numerical results show the actual implementation of the method with noiseless or noisy data simulated data derived from the FEM.

To be able to effectively demonstrate our method without excessively computational efforts, we choose $N = 4$ and probe the region from the top and the bottom boundaries in the numerical simulation. It is of course very natural to choose large N and also probe the region from all sides. However, obtaining the simulated data for this improvement will be a very time-consuming task.

From the numerical results, our method is very effective in determining parts of the object near the boundary even when the domain is unbounded. Its flexibility gives us another technique that can potentially be used in real applications such as medical imaging and nondestructive evaluation.

Appendix A

In this appendix, we show how to implement the artificial boundary condition (4.6) in the FEM. Denote $u = (u_1, u_2)^T$. Let Γ_D be the boundary with imposed Dirichlet data $f_{N,t,h}$ and Γ_A denote the artificial boundary.

From the variational formulation of Eq. (1.2), the isotropic elastic system on the truncated domain in Section 4.3 can be written as follows:

$$\begin{aligned} & \int_{\Omega} \begin{pmatrix} \partial_1 v_1 \\ \partial_2 v_2 \\ \partial_2 v_1 + \partial_1 v_2 \end{pmatrix}^T \begin{pmatrix} \lambda + 2\mu & \lambda & 0 \\ \lambda & \lambda + 2\mu & 0 \\ 0 & 0 & \mu \end{pmatrix} \begin{pmatrix} \partial_1 u_1 \\ \partial_2 u_2 \\ \partial_2 u_1 + \partial_1 u_2 \end{pmatrix} dx \\ & - \int_{\partial\Omega} v_1 (\lambda \nabla \cdot u + 2\mu \partial_1 u_1, \mu (\partial_2 u_1 + \partial_1 u_2)) \cdot \mathbf{n} ds \\ & - \int_{\partial\Omega} v_2 (\mu (\partial_2 u_1 + \partial_1 u_2), \lambda \nabla \cdot u + 2\mu \partial_2 u_2) \cdot \mathbf{n} ds = 0, \end{aligned} \quad (\text{A.1})$$

where v_1, v_2 are test functions in $H_{0, \Gamma_D}^1(\Omega) = \{v \in H^1(\Omega) \mid v(x) = 0 \text{ for } x \in \Gamma_D\}$. From (4.6), one has that

$$\partial_1 u_1 + \partial_2 u_2 = \nabla \cdot u = 0 \quad \text{and} \quad \partial_1 u_2 - \partial_2 u_1 = 0, \quad (\text{A.2})$$

on Γ_A . Since the artificial boundary consists of line segments along the x_2 -direction only, by (A.2), the partial derivatives $\partial_1 u_1$ and $\partial_1 u_2$ are replaced by $-\partial_2 u_2$ and $\partial_2 u_1$, respectively. Thus the variational formulation (A.1) becomes:

$$\begin{aligned} & \int_{\Omega} \begin{pmatrix} \partial_1 v_1 \\ \partial_2 v_2 \\ \partial_2 v_1 + \partial_1 v_2 \end{pmatrix}^T \begin{pmatrix} \lambda + 2\mu & \lambda & 0 \\ \lambda & \lambda + 2\mu & 0 \\ 0 & 0 & \mu \end{pmatrix} \begin{pmatrix} \partial_1 u_1 \\ \partial_2 u_2 \\ \partial_2 u_1 + \partial_1 u_2 \end{pmatrix} dx \\ & + \int_{\Gamma_A} 2\mu v_1 (\partial_2 u_2, -\partial_2 u_1) \cdot \mathbf{n} dx_2 - \int_{\Gamma_A} 2\mu v_2 (\partial_2 u_1, \partial_2 u_2) \cdot \mathbf{n} dx_2 = 0. \end{aligned} \quad (\text{A.3})$$

As a result, the standard finite element discretization procedure can now be employed in (A.3).

References

- [1] H. Ammari, H. Kang, Polarization and Moment Tensors: With Applications to Inverse Problems and Effective Medium Theory, Applied Mathematical Sciences, vol. 162, Springer, 2007.
- [2] H. Ammari, H. Kang, G. Nakamura, K. Tanuma, Complete asymptotic expansions of solutions of the system of elastostatics in the presence of an inclusion of small diameter and detection of an inclusion, J. Elasticity 67 (2002) 97–129.
- [3] H. Ammari, P. Garapon, H. Kang, H. Lee, A method of biological tissues elasticity reconstruction using magnetic resonance elastography measurements, Quart. Appl. Math. 66 (2008) 139–175.
- [4] A.P. Calderón, On an inverse boundary value problem, in: Seminar on Numerical Analysis and its Applications to Continuum Physics, Rio de Janeiro, 1980.
- [5] H. Heck, G. Uhlmann, J.-N. Wang, Reconstruction of obstacles immersed in an incompressible fluid, Inverse Problems and Imaging 1 (2007) 63–76.
- [6] T. Ide, H. Isozaki, S. Nakata, S. Siltanen, G. Uhlmann, Probing for electrical inclusions with complex spherical waves, Comm. Pure Appl. Math. 60 (2007) 1415–1442.
- [7] M. Ikehata, Size estimate of inclusion, J. Inverse Ill-Posed Probl. 6 (1998) 127–140.
- [8] M. Ikehata, Reconstruction of inclusion from boundary measurements, J. Inverse Ill-Posed Probl. 10 (2002) 37–65.
- [9] M. Ikehata, A remark on an inverse boundary value problem arising in elasticity, preprint.
- [10] M. Ikehata, Inverse conductivity problem in the infinite slab, Inverse Probl. 17 (2001) 437–454.
- [11] M. Ikehata, Mittag-Leffler's function and extracting from Cauchy data, in: Inverse Problems and Spectral Theory, in: Contemp. Math., vol. 348, Amer. Math. Soc., Providence, RI, 2004, pp. 41–52.
- [12] M. Ikehata, S. Siltanen, Electrical impedance tomography and Mittag-Leffler's function, Inverse Probl. 20 (2004) 1325–1348.
- [13] V. Isakov, On uniqueness of recovery of a discontinuous conductivity coefficient, Comm. Pure Appl. Math. 41 (1988) 865–877.
- [14] H. Kang, E. Kim, J.Y. Lee, Numerical reconstruction of a cluster of small elastic inclusions, Inverse Probl. 23 (2007) 2311–2324.
- [15] G. Nakamura, G. Uhlmann, Global uniqueness for an inverse boundary problem arising in elasticity, Invent. Math. 118 (1994) 457–474.
- [16] M. Salo, J.-N. Wang, Complex spherical waves and inverse problems in unbounded domains, Inverse Probl. 22 (2006) 2299–2309.
- [17] G. Uhlmann, Developments in inverse problems since Calderón's foundational paper, in: Harmonic Analysis and Partial Differential Equations (Essays in Honor of Alberto P. Calderón), The University of Chicago Press, Chicago, 1999, pp. 295–345.
- [18] G. Uhlmann, Commentary on Calderón's paper (29), On an inverse boundary value problem, in: A. Bellow, C.E. Kenig, P. Malliavin (Eds.), Selected Papers of Alberto P. Calderón with Commentary, AMS, 2008, pp. 623–636.
- [19] G. Uhlmann, J.-N. Wang, Complex spherical waves for the elasticity system and probing of inclusions, SIAM J. Math. Anal. 38 (2007) 1967–1980.
- [20] G. Uhlmann, J.-N. Wang, Reconstructing discontinuities using complex geometrical optics solutions, SIAM J. Appl. Math. 68 (2008) 1026–1044.